STRUCTURAL FEATURES AND SURFACE HEAT TRANSFER ASSOCIATED WITH A ROW OF SHORT-HOLE JETS IN CROSSFLOW

Charles A. Hale, Michael W. Plesniak, & Satish Ramadhyani
School of Mechanical Engineering, Purdue University
Maurice J. Zucrow Laboratories
West Lafayette, IN 47907-1288, USA

ABSTRACT

Surface streak experiments coupled with flow visualization and numerical simulations were used to investigate short length-to-diameter injection holes for geometries of interest to the gas turbine industry. The flow field results were also related to measured surface heat transfer in the downstream region of the jets. Geometric surface topology maps inferred from "oil and lampblack" surface streak experiments give insights into the flow field, as well as boundary layer disruption, and ultimately the convective heat transfer coefficient enhancement in the wake region of the jets.

A secondary counter-rotating vortex pair (CRVP) with the opposite sense of rotation as the well documented main counter-rotating vortex pair is found to enhance the attachment event in the wake region and correspondingly increase the center line enhancement of the convective heat transfer coefficient. In addition to providing information about the crossflow boundary layer disruption, the surface topological results relate the signature of the surface shear stress to the coherent flow structures in the flow field being investigated.

INTRODUCTION

Demands for higher thermal efficiencies in modern gas turbines have prompted designers to steadily increase first-stage gas inlet temperatures to a level that necessitates aggressive cooling schemes. Turbine inlet temperatures of 1900 K are typical of current designs, and there is interest in elevating the temperatures even higher. Such temperatures are well above the failure temperature of the blade material.

One method of protecting airfoils in these harsh environments is discrete-hole film cooling. Cooler, denser air is bled from the compressor and fed through internal passages in the blade or vane. The coolant then flows from the internal passages and impinges on the internal surface of the blade before turning to flow through a narrow internal plenum. From the supply plenum, the coolant is injected through small discrete holes into the external boundary layer forming a protective film on the surface. Prediction of discrete-hole film-cooling performance requires and improved understanding of the fundamental jet-in-crossflow. The jet-in-crossflow has been studied extensively for over fifty-five years, as discussed in a review paper by Margason (1993). However, many issues remain unresolved as reported recently by Morton and Ibbetson (1996), Haven and Kurosaka (1997), Kelso *et al.* (1998), Fric and Roshko (1994), Findlay *et al.* (1997), Yuan and Street (1998), Smith and Mungal (1998), and Brizzi *et al.* (1997).

The current investigation examines the effects of plenum and injection hole geometry on discrete-hole film cooling performance. The objective was to relate the hydrodynamics and structural features of the flow field associated with a row of jets-in-crossflow to the surface heat transfer performance. The results are applicable to current advanced design interest for first stage vanes in which the thin wall thickness results in length-to-diameter ratios (L / D) < 3. Under these conditions, the flow exiting the coolant hole is far from fully developed and there is strong coupling between the coolant supply and the external crossflow.

EXPERIMENTAL APPARATUS AND TECHNIQUES

Experimental studies were conducted in a low-speed wind tunnel with a 122 cm long by 30 cm square, optically clear test section with a single row of injection holes on a flat plate. A specially-designed section allows the injection hole length-to-diameter ratio to be varied as well as the direction of the flow in the plenum, which feeds the film cooling holes. The experimental study utilizes high-speed flow visualization, surface streaking experiments, and liquid crystal surface heat transfer measurements.

In order to measure the convective surface heat transfer coefficient (h) a thin film heater consisting of two copper buss bars spanning the streamwise length of the heater and a 0.0254 mm thick piece of stainless steel acting as the resistor was placed into an adiabatic floor constructed from extruded polystyrene (k = 0.026 W / m K). A schematic of the thin film heater is shown in Figure 1. The stainless steel heater provided constant heat flux (q") over its surface area when supplied with current from a power supply with 800 amp capability. The heater surface was coated with cholesteric liquid crystal paint (*Hallcrest* 28c1W) on a flat black background. The mass flow rate of the injection air was monitored by the orifice plate flow meter with an embedded thermocouple to account for changes in air density with temperature. The crossflow freestream velocity was monitored using a pitot-static tube measuring the dynamic head with a micro-manometer with a resolution of 0.025 mm of water. The blowing ratios were calculated based on the plug flow jet-exit velocity associated with the total jet injection mass flow rate.

The jet temperature was maintained at the freestream temperature using a constant temperature bath flowing through a compact heat exchanger at the inlet of the secondary injection blower. During the experiments different surface heat flux values, and therefore different h values, were set by adjusting the current to the heater.

The constant heat flux value was calculated using the measured dimensions of the heater and the resistivity of the heater material and the measured current.

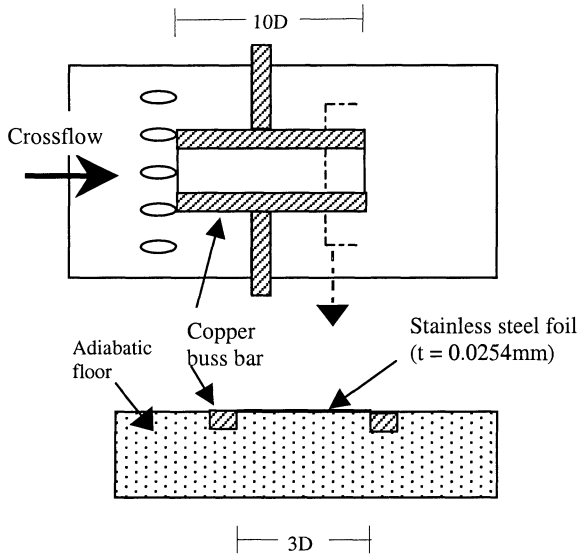

Figure 1. Adiabatic floor containing heater

The experimental uncertainties were 6% for the blowing ratio and 6 to 9 % for the convective heat transfer coefficient (Hale, 1999). First order corrections were also made to the surface temperature measurements to account for radiation and conjugate effects. The conjugate effects were modeled numerically.

A *Cooke Flashcam* was used to capture 20 to 40 μs duration exposures of the flowfield, while a *Redlake MotionScope HR2000* high-speed digital camera capable of framing rates of 2000 fps was used to examine the temporal evolution of the flow.

The surface streak experiments were performed by attaching white contact paper to the injection plate region, coating the surface with a tracer and recording the resulting pattern after the tunnel was operated. The streaks are created using the "oil and lampblack" method. Lampblack is not readily available, therefore another substance was sought. The mixture found to work after many trial and error iterations is: 1 part copier toner, 2 parts kerosene-based *Fog Juice*, and 7 parts baby oil. This mixture worked well for the current velocity field, but would need to be optimized for other flow conditions. Once the mixture was applied, the wind tunnel and secondary blower were turned on simultaneously. The ensuing transient behavior was recorded with a *Canon ES 1000* 8mm video camera. At steady state the surface streak pattern was recorded (photographed) using a *Nikon FM2* camera. For the flow visualization and surface streak experiments polycarbonate downstream floors and injection plates rather than polystyrene were used (see Figure 2) and the blowing ratio and freestream velocity were measured in the same manner as for the heat transfer experiments.

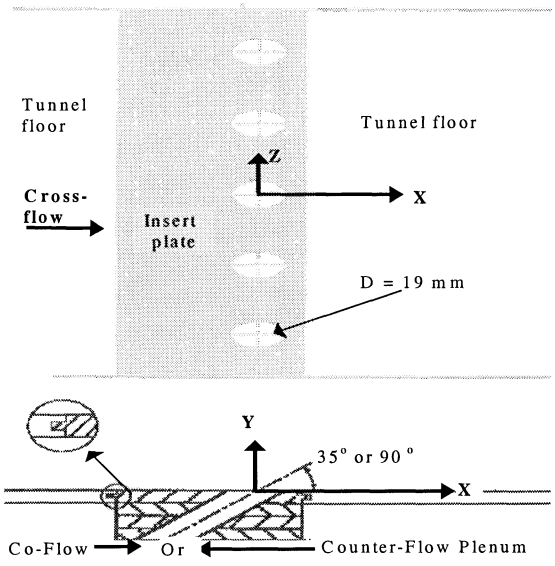

Figure 2. Variable-thickness injection plates installed in the tunnel floor

The experimental parameters investigated in the current study are presented in Table 1. While the scaled geometric parameters are of interest to the gas turbine industry, the

conditions do not replicate realistic density ratios, freestream turbulence levels, Mach numbers, or surface curvature associated with real engine conditions.

Table 1. Parameters Studied

Hole diameter (D)	19 mm
Number of holes	5
Hole spanwise spacing (P / D)	3
Free stream velocity (U_∞)	10 m/s
Blowing ratio ($M = \rho_j u_j / \rho_\infty U_\infty$)	0.5, 1.0, 1.5
Hole length-to-diameter ratio (L / D)	0.66, 3.0 (90° jets)
	1.16, 2.91 (35° jets)
Plenum feed direction	co-flow, counter-flow
Plenum height	1D
Endwall distance (E / D)	1 (35° jets)
	0.66 (90° jets)
B.L. Displacement thickness (δ^* / D)	0.1 to 0.15
B.L. Momentum thickness (θ / D)	0.09
B.L. Reynolds numbers (Re_θ)	1024
(Re_δ)	10,500
(Re_{δ^*})	1428
(Re_x)	1.4×10^6
Jet Reynolds number (Re_D)	12,000 (M = 1.0)

NUMERICAL TECHNIQUES

The computations were performed on an IBM RS 6000 workstation with 512 megabytes of random access memory. The commercial software package GeoMesh was used to generate the geometry and mesh. The domain includes the narrow plenum, the injection hole, and the crossflow region. The structured body-fitted mesh was created using the object-oriented, parametric block modeling tool P-Cube contained in the GeoMesh package. The grid was generated by specified node bunching using Eriksson interpolation schemes and was also smoothed using Thomas-Middlecoff relaxation schemes. An example of the computational domains created is shown in Figure 3, and the near-hole grid at the jet exit plane is shown in Figure 4. Symmetry planes at the center line of the hole and the mid-plane between adjacent holes were used to reduce the number of cells.

The low Mach number, Reynolds-Averaged Navier-Stokes equations were solved using second-order upwind discretization schemes and various turbulence models and near-wall-treatment. This formulation allows the simulation of the effects of differences in density arising from temperature differences in the two streams. The k-ε, RNG k-ε, and Reynolds Stress turbulence models were examined. Non-equilibrium wall functions and two-layer zonal models were used for near-wall-treatment. These turbulence models and near-wall-treatment methods, as implemented by FLUENT, are discussed in detail by Ferguson *et al.* (1998) and Hale (1999) and the theory is presented in an extensive set of user manuals available with the FLUENT software (FLUENT, 1997).

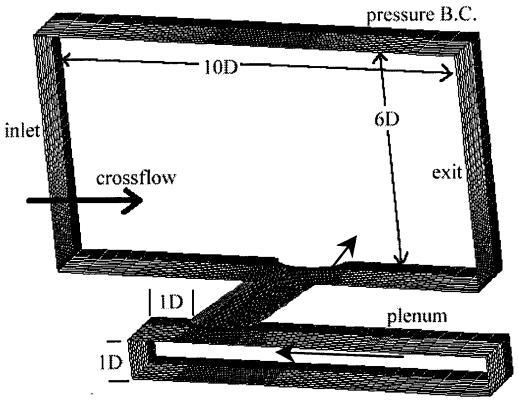

Figure 3. Computational domain

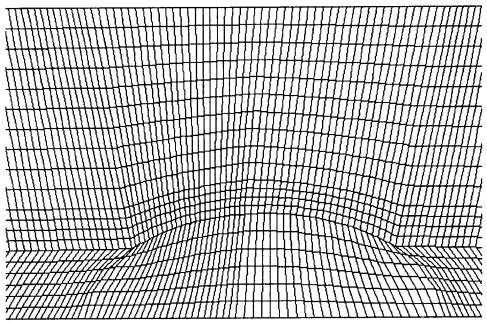

Figure 4. Top view of near-hole grid distribution (1/2 grid density shown for clarity)

Most cases required grids containing approximately 600,000 cells using wall functions and 900,000 cells when using the two-layer zonal near wall treatment. Grid independence was achieved when the predicted centerline effectiveness and jet exit velocity profiles changed by less than 0.1% with increased grid density. The grid independence studies were performed for fixed y^+ values of the wall-adjacent cells. These y^+ values were approximately 1 and 25 for the two-layer zonal model and wall function formulations, respectively.

The ability of the different turbulence models to predict current heat transfer data and published hydrodynamic and heat transfer data for geometries similar to the current study (e.g. Pietrzyk *et al.*, 1990 and Sinha *et al.* 1991) were evaluated and it was concluded that the Reynolds Stress model coupled with the two-layer zonal model near wall treatment gave the best results. All numerical results presented here were obtained using the Reynolds Stress-two-layer-zonal model. Detailed comparisons of the turbulence models are presented in Hale *et al.* (1999).

The assumed symmetry and time-averaging are two limitations of the simulations. Recent work by Smith and Mungal (1998) and Cusano and Plesniak (1999) shows that the jet-in-crossflow structures are unsteady and asymmetric (in the mean) under certain conditions. However the

simulations were adequate to yield insight regarding the role of coherent structures on the measured surface streaklines and heat transfer coefficient data.

RESULTS

A large parameter space was explored in the study, but only the results of a couple of configurations will be discussed due to space limitations. Complete details are available in Hale (1999). Figures 5 (a) and (b) show the results of the surface streak experiments for two cases explored. The cases will be referred to as "90° short co-flow" and "90° short counter-flow", respectively. Recall that all cases studied consisted of short injection holes, here the term "short" refers to the shorter injection holes studied during the parametric study (L / D = 0.66). The topology maps inferred from the surface streak data are presented in Figures 6 (a) and (b). It is obvious that the change in the plenum-flow direction affects the flow field and therefore the resulting surface topological map. The geometric surface topological rules used to evaluate the possible flow fields are consistent with those reported by Lighthill (1963), Hunt *et al.* (1978), Tobak and Peake (1979), Chapman (1986), Unal (1988), and Davis (1990). A complete discussion of applications of geometric surface topology to surface streak data is given in Hale (1999).

The Euler characteristic, $X(M) = \sum nodes - \sum saddles$, for the region in Figure 5 is -1. Caution must be used in evaluating the Euler characteristic of the jet-in-crossflow region, because critical points on the surface map can be inside the injection hole if separation or recirculation exist inside the hole.

The upstream node-saddle pairs correspond to the horseshoe vortices captured in the flow visualization and the numerical study shown in Figure 7 (a) and (b), respectively. In all cases investigated, the horseshoe vortices were found to be weak structures that dissipate quickly.

The spiral nodes in the downstream region correspond to the time-averaged separation related to the wake vortices. The signature location of the vortices is different in the two cases. There is one pair of nodes ($N_{1\ \&\ 2}$) for the co-flow plenum case and two pairs ($N_{3,4\ \&\ 5,6}$) of separation nodes in the counter-flow plenum case. Both cases have an attachment region in the wake region of the jet: N_3 for the co-flow case and N_7 in the counter-flow case. It is expected that the convective heat transfer coefficient will increase in a region of attachment.

The separation along the separatrix connecting the saddle point to the nodes of separation, saddle points $S_{5,6\ \&\ 7,8}$ for the counter-flow case and $S_{3,4}$ for the co-flow plenum configuration, is consistent with the separation event discussed by Fric and Roshko (1994). A numerically predicted region of low pressure that contains an in-hole vortex connected to the time-averaged wake vortex is shown in Figure 8. The region surrounded by the constant pressure surface on the wall in the wake region is clearly seen in the surface streaks downstream of the jet (refer to Figure 5).

The shape of the constant pressure surface suggests that the wake vortex and the counter-rotating vortex pair are strongly coupled with the vorticity inside the hole and the vorticity at the jet-crossflow interface near the edge of the hole. The predicted velocity field in the near-wall region agrees well with the topology maps inferred from the surface streak experiments.

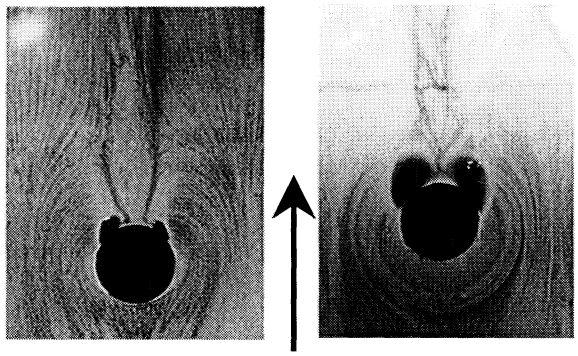

Crossflow

(a) co-flow plenum (b) counter-flow plenum

Figure 5. Surface streaks surrounding interior jet for 90° short cases at M = 1.0

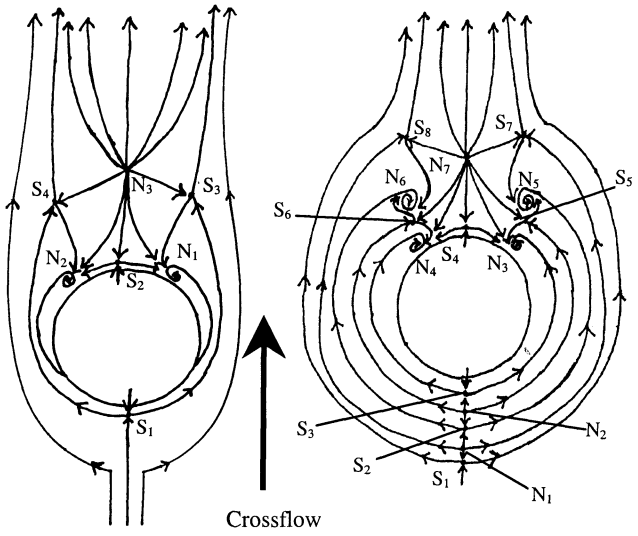

(a) co-flow plenum (b) counter-flow plenum

Figure 6. Topology maps for 90° short cases at M = 1.0

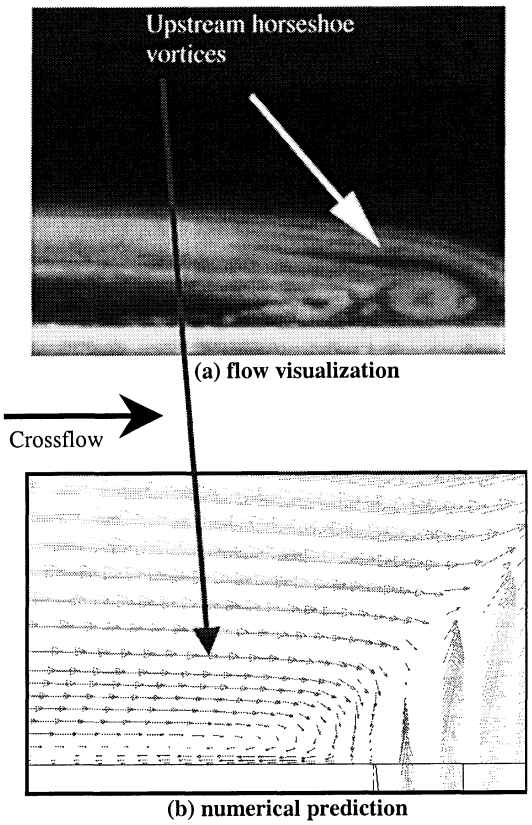

Figure 7. Upstream horseshoe vortices

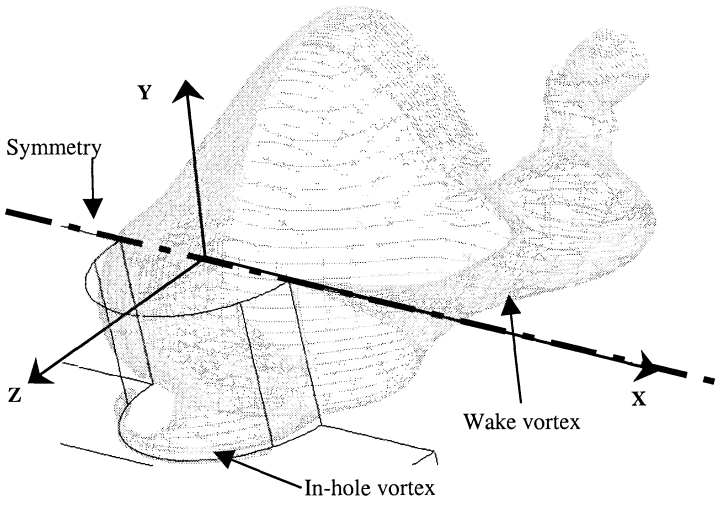

Figure 8. Numerically predicted constant pressure surface

The surface streaks and topology maps show that the attachment region along the centerline of the jet does not contain the expected line of separation which would be associated with the sense of rotation of the primary counter-rotating vortex pair (CRVP). The complementary numerical simulations explain the observed topological map. The simulations revealed the presence of a secondary CRVP located below the primary pair and with the opposite sense of rotation. Secondary pairs have been reported but are not well-documented in the literature, and they are difficult to visualize experimentally. Figure 9 (a) shows the cross plane velocity vectors with the main flow coming out of the page. Only one half of the pair is shown about the plane of symmetry. Figure 9 (b) shows the magnified view of the second CRVP.

Figure 10 shows the contours of constant surface heat transfer coefficient (h). The counter-flow data are presented on the upper half of the plot, while the co-flow data are presented on the lower half of the figure so that side by side comparisons may be made. Referring to Figure 6, the region of attachment is larger for the co-flow plenum; corresponding to a stronger secondary CRVP and more center-line heat transfer coefficient enhancement (iso-h lines pushed downstream) as seen along the centerline region in Figure 10. The topology maps also show that the boundary layer is more disrupted for the counter flow case. This is expected to increase the magnitude of the convective heat transfer coefficients in the downstream region and affect a larger spanwise region downstream of the injection holes. These trends are evident when the extent of the spanwise affected region and relative h magnitudes are compared.

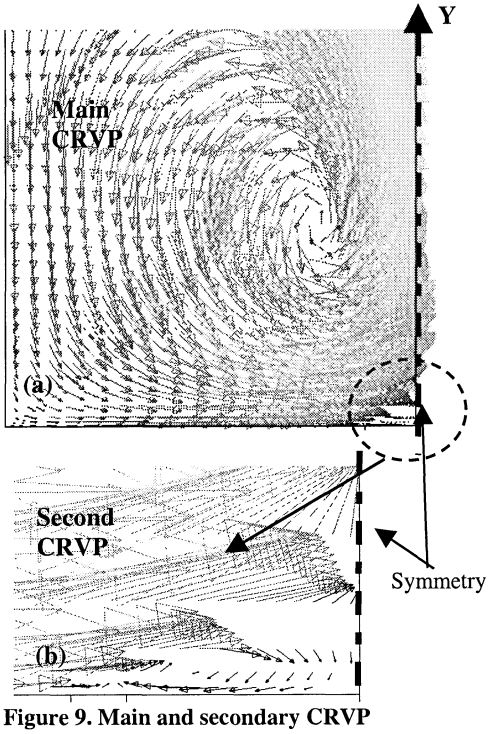

Figure 9. Main and secondary CRVP

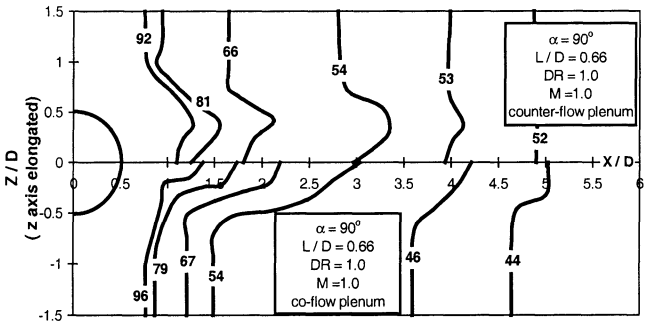

Figure 10. Convective heat transfer coefficient contours (h [W / m^2 K]) for short hole 90° cases at M = 1.0

CONCLUSIONS

The structures associated with a row of "short-hole" jets injected into a crossflow have been identified experimentally and computed numerically. The existence of a secondary counter-rotating vortex pair located closer to the wall than the main pair was inferred from the surface topological map and numerical predictions. The second pair is stronger for the co-flow case, resulting in strong centerline enhancement of the heat transfer coefficient. The increased disruption of the boundary layer for the counter-flow case resulted in higher spatially-averaged heat transfer coefficient values in the downstream region of the jet.

The use of geometric surface topology revealed the signatures of the horseshoe structures, boundary layer separation, the time-averaged wake vortices, and the secondary CRVP. Combining the topological maps and the surface heat transfer data, enables relatively simple surface streak experiments to qualitatively predict heat transfer enhancement or degradation during parametric studies. The numerical solutions also suggest that the vorticity associated with the wake vortices and the main CRVP are strongly related to the vorticity inside the hole and the vorticity at the jet-crossflow interface near the edge of the hole. With further investigation, the full field data available in the numerical solutions have the potential to give more insight into the time-averaged structure of the flow field, which is of interest to the gas turbine industry.

ACKNOWLEDGEMENTS

We gratefully acknowledge the sustained support of Rolls-Royce/Allison Engine Co. C.A. Hale was supported by Purdue Research Foundation and Ingersoll-Rand fellowships during the course of this research.

REFERENCES

Brizzi, L., Foucault, E., Bernard, A., and Bousgarbles, J., 1997, "In the Vicinity of a Jet in a Cross-flow," ASME Paper FEDSM97-3083.

Chapman, G.T., 1986, "Topological Classification of Flow Separation on Three-dimensional Bodies," AIAA Paper 86-0485.

Cusano, D.M., and Plesniak, M.W., 1999, "Asymmetry in a Confined Rectangular Jet in Crossflow," Proceedings of the First Symposium on Turbulent Shear Flow Phenomena.

Davis, R.E., 1990, "Secondary Flow and Three-dimensional Separation in Curved Circular Ducts," Ph.D. Thesis, School of Aeronautical Engineering, Purdue University.

Ferguson, J.D., Walters D.K. and Leylek, J.H., 1998, "Performance of Turbulence Models and Near-Wall Treatments in Discrete Jet Film Cooling Simulations," ASME Paper 98-GT-438.

Findlay, M.J., Salcudean, M., and Gartshore, I.S., 1997, "Jets in a Crossflow: Effects of Geometry and Blowing Ratio," ASME Paper FEDSM97-3299.

FLUENT INC., 1997, FLUENT User's Guide.

Fric, T.F. and Roshko, A. 1994, "Vortical Structure in the Wake of a Transverse Jet," *Journal of Fluid Mechanics,* **279**, 1-47.

Hale, C.A., 1999, "Short Hole Film Cooling Hydrodynamics and Convective Heat Transfer in the Near-hole Region," Ph.D. Thesis, School of Mechanical Engineering, Purdue University.

Hale, C.A., Ramadhyani, S.,and Plesniak, M.W.,1999, "Film Cooling Effectiveness Predictions for Short Holes Fed by a Narrow Plenum," ASME TURBO EXPO 1999.

Haven, B.A. & Kurosaka, M., 1997, "Kidney and Anti-kidney Vortices in Crossflow Jets," *Journal of Fluid Mechanics*, **352**, 27-64.

Hunt, J.C.R., Abell, C.J., Peterka, J.A., and Woo, H., 1978, "Kinematical Studies of the Flows Around Free or Surface-mounted Obstacles: Applying topology to Flow Visualization," *Journal of Fluid Mechanics*, **86**, part 1, 179-200.

Kelso, R.M., Lim, T.T., and Perry, A.E., 1998, "New Experimental Observations of Vortical Motions in Transverse Jets," *Physics of Fluids*, **10,** Num. 9, 2427-2429.

Lighthill, M.J., 1963, Chapters 1 and 2 of, *Laminar Boundary Layers*, as presented in *Collected Papers of Sir James Lighthill Volume II*, Edited by M. Yousuff Hussaini, Oxford University Press, 1997.

Margason, R.J., 1993, "Fifty Years of Jet in Cross Flow Research," AGARD-CP-534 Nov. 1993.

Morton, B.R. and Ibbetson, A., 1996, "Jets Deflected in a Crossflow," *Experimental Thermal and Fluid Science,* **12**, 112-133.

Pietrzyk, J.R., Bogard, D.G., and Crawford, M.E., 1990, "Effects of Density Ratio on the Hydrodynamics of Film Cooling," *Journal of Turbomachinery,* **112**, 437-443.

Sinha, A.K., Bogard, D.G., and Crawford, M.E., 1991b, "Film-Cooling Effectiveness Downstream of a Single Row of Holes With Variable Density Ratio," *Journal of Turbomachinery*, **113**, 442-449.

Smith, S.H. and Mungal, M.G., 1998, "Mixing, Structure and Scaling of the Jet in Crossflow," *Journal of Fluid Mechanics*, **357**, 83-122.

Tobak, M., and Peake, D.J., 1979, "Topology of Two-dimensional and Three-dimensional Separated Flows," AIAA Paper 79-1480.

Unal, A., 1987, "Three-dimensional Singular Points in Aerodynamics," NASA TM-100045, USAAVSCOM TR-87-A-14.

Yuan, L.L. and Street, R.L., 1998, "Trajectory and Entrainment of a Round Jet in Crossflow," *Physics of Fluids*, **10,** Num. 9, 2323-2335.